HAL open science

Rational approach for an optimized formulation of silver-exchanged zeolites for iodine capture from first-principles calculations

Tarek Ayadi, Michael Badawi, Laurent Cantrel, Sébastien Lebègue

▶ **To cite this version:**

Tarek Ayadi, Michael Badawi, Laurent Cantrel, Sébastien Lebègue. Rational approach for an optimized formulation of silver-exchanged zeolites for iodine capture from first-principles calculations. Molecular Systems Design & Engineering, 2022, 7 (5), pp.422-433. 10.1039/d1me00149c . irsn-04111809

HAL Id: irsn-04111809

https://irsn.hal.science/irsn-04111809v1

Submitted on 31 May 2023

HAL is a multi-disciplinary open access archive for the deposit and dissemination of scientific research documents, whether they are published or not. The documents may come from teaching and research institutions in France or abroad, or from public or private research centers.

L'archive ouverte pluridisciplinaire **HAL**, est destinée au dépôt et à la diffusion de documents scientifiques de niveau recherche, publiés ou non, émanant des établissements d'enseignement et de recherche français ou étrangers, des laboratoires publics ou privés.

Distributed under a Creative Commons Attribution - NonCommercial 4.0 International License

Volume 7
Number 5
May 2022
Pages 405–530

MSDE

Molecular Systems Design & Engineering

rsc.li/molecular-engineering

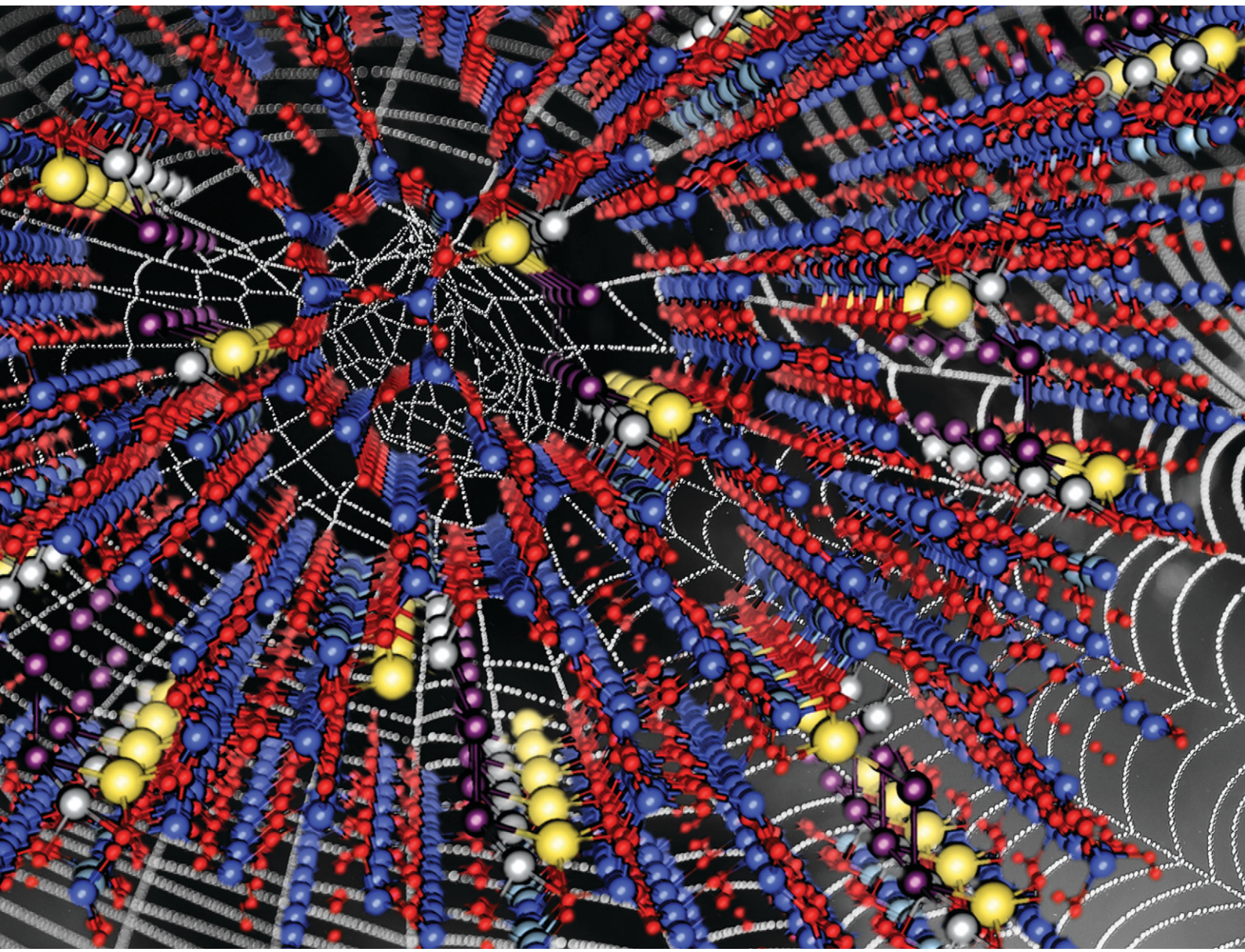

ISSN 2058-9689

ROYAL SOCIETY OF CHEMISTRY

PAPER

Michael Badawi *et al.*

Rational approach for an optimized formulation of silver-exchanged zeolites for iodine capture from first-principles calculations

IChemE ADVANCING CHEMICAL ENGINEERING WORLDWIDE

MSDE

PAPER

View Article Online
View Journal | View Issue

Open Access Article. Published on 03 February 2022. Downloaded on 5/31/2023 10:42:03 AM.
This article is licensed under a Creative Commons Attribution-NonCommercial 3.0 Unported Licence.

Check for updates

Cite this: *Mol. Syst. Des. Eng.*, 2022, 7, 422

Rational approach for an optimized formulation of silver-exchanged zeolites for iodine capture from first-principles calculations

Tarek Ayadi,[a] Michael Badawi,*[a] Laurent Cantrel[b] and Sébastien Lebègue[a]

Received 18th October 2021,
Accepted 21st January 2022

DOI: 10.1039/d1me00149c

rsc.li/molecular-engineering

Ab initio calculations have been carried out to investigate in detail the effect of potential inhibiting species (CO, H_2O, CH_3Cl and Cl_2) on the adsorption of iodine species (I_2 and CH_3I) in silver-exchanged zeolites of different Si/Al ratios and structures (faujasite, mordenite, chabazite and clinoptilolite). We have found that the adsorption of iodine species becomes more favorable for a low Si/Al ratio. Indeed, a potentially strong inhibiting effect of CO for a high Si/Al ratio has been unravelled, while Cl_2 appears as an inhibitor for a low Si/Al ratio. In addition, a spontaneous dissociation is observed for I_2 and Cl_2 at a low Si/Al ratio which greatly increases the interaction energy. With the addition of sodium cations together with the silver ones to compensate for the charge in the zeolite structures, an improvement in the performance of mordenite for the selective trapping of iodine compounds is observed, in contrast to chabazite and clinoptilolite. Interestingly, we found that the presence of the Na cations in faujasite and mordenite prevents the spontaneous dissociation of the Cl_2 molecule, which leads to limitation of the strong inhibiting effect on the adsorption of iodine species, in particular CH_3I. Also, an efficient comparison between different structures using radar charts has been performed, where not only the Si/Al ratio is taken into consideration but also the silver loading in the zeolite structure for a given Si/Al ratio. Finally, we found that Ag-chabazite with a Si/Al of 5 and AgNa-mordenite with a Si/Al of 11 are the best candidates for selective trapping of iodine species, noticeably for I_2 trapping.

Design, System, Application

The trapping of harmful iodine species as released during a nuclear accident can be achieved using silver zeolites. However, a large experimental study of many different zeolite structures and Si/Al ratios to find the best formulation would be extremely time consuming. Here, we have employed density functional theory to investigate systematically the performance of different silver-exchanged zeolites, with the aim to propose an optimized formulation that can be experimentally tested.

1 Introduction

Since the Fukushima nuclear accident, great effort has been given by the scientific community to mitigate dangerous radioactive compounds before they reach the environment. In particular, iodine species attract specific interest among radiotoxic releases because the ^{131}I isotope can contribute significantly to the radiological consequences in the short term.[1–3] To confine these species and limit their effect in the environment, a specific filtration device on the CVS, selective towards iodine species, is recommended. Among the most efficient technologies that can be used to improve iodine filtration (I_2 and CH_3I) are those based on zeolites.[4–9] Together with iodine species, different potential species are formed during severe nuclear accidents with different concentrations, which can inhibit iodine trapping. We mainly find large amounts of steam (40–90%) and other gaseous compounds such as CO, CH_3Cl and Cl_2.[10,11] The CO compound comes from the molten core concrete interactions which start after vessel rupture, while chlorine compounds (CH_3Cl and Cl_2) are produced by fuel fission as well as possible thermal degradation of cables.[12,13]

Zeolites are a family of porous adsorbent materials.[14–17] Usually, zeolite structures are formed mainly by three dimensional microporous frameworks comprising channels and voids made up of tetrahedral silicon and aluminum atoms bonded to oxygen atoms. These crystals have interesting characteristics such as high thermal stability, the

[a] *Laboratoire Physique et Chimie Théoriques (LPCT, UMR CNRS UL 7019), Institut Jean Barriol, Université de Lorraine, BP 239, Boulevard des Aiguillettes, 54506 Vandoeuvre-lès-Nancy Cedex, France. E-mail: michael.badawi@univ-lorraine.fr*
[b] *Institut de Radioprotection et de Sûreté Nucléaire, PSN-RES, CEA Cadarache, F-13115 Saint Paul lez Durance, France*

This journal is © The Royal Society of Chemistry and IChemE 2022

Open Access Article. Published on 03 February 2022. Downloaded on 5/31/2023 10:42:03 AM.
This article is licensed under a Creative Commons Attribution-NonCommercial 3.0 Unported Licence.

ability to exchange ions, high specific surface area, and large pores and cages. With these remarkable properties, zeolites proved their performance in various applications as cleaners, gas filters, catalysts and agents for treatment of nuclear wastes.[5,7,18,19] Indeed, there are many types of zeolites with different structural frameworks such as faujasite, mordenite, chabazite and clinoptilolite.[5,7] This diversity leads to different properties, which widens the field of applications.

Cation exchange is a result of the replacement of Si atoms by Al atoms in the zeolite structures where a negative charge is produced. This exchange is one of the most important parameters where the properties of the zeolite can vary depending on the type of cation used to compensate for the charge in the structure. Theoretical and experimental studies have shown that silver is the most efficient cation among various metals (Cu, Na, Pb, Tl, Cd) for iodine species trapping by the formation of AgI precipitates.[6,17,20–24] For an in-depth understanding of this phenomenon, an experimental study has been carried out by Azambre and Chebbi[24] on different Ag-exchanged zeolites (faujasite X and Y, mordenite, *BEA, MFI, FER) to understand the relationships between the structural and chemical parameters and the efficiency for iodine trapping (CH_3I). They found that the formation of AgI for all Ag exchanged zeolites and the amount of AgI precipitates are directly related to the silver loading in the structure. Formation of silver clusters can also occur in zeolites[25] but recent experimental studies have demonstrated that isolated silver cations can be well inserted into zeolites by cationic exchange even at high silver loading (up to 23%).[24] For this cation loading which corresponds to a low Si/Al ratio, no blocking of channels has been observed.[24]

In order to find the best silver exchanged zeolitic formulation owing the good compromise between the selective trapping of iodine species towards inhibitor species (CO, H_2O, CH_3Cl and Cl_2) and the silver amount, we have investigated the potential impact of CO, H_2O, CH_3Cl and Cl_2 on iodine trapping for silver exchanged faujasite, mordenite, chabazite and clinoptilolite. During our study, we took into consideration not only the Si/Al ratio but also the silver content in the structure where the Na cations are introduced to compensate for the charge together with the Ag ones.

The paper is organized as follows: first, we detail our computational procedure, then the obtained results with Ag-faujasite, mordenite, chabazite and clinoptilolite for several Si/Al ratios are presented and discussed with a focus on the potential inhibiting effect of CO, H_2O, CH_3Cl and Cl_2 on the trapping of iodine species, and finally we outline the main conclusions of our study.

2 Computational details

We have performed *ab initio* calculations by means of density functional theory (DFT) with the projector augmented wave (PAW) method[26] as implemented in the Vienna *ab initio* simulation package (VASP).[27] For the exchange and correlation contributions, the Perdew–Burke–Ernzerhof (GGA-PBE) functional[28] was employed with a kinetic energy cutoff of 450 eV for the plane wave basis set. The correction of Tkatchenko–Scheffler with iterative Hirshfeld partitioning (TS/HI)[29,30] was used to describe dispersion interactions. Recently, this method has proved its performance for describing adsorption phenomena on zeolites owing to its capacity to properly describe ionic systems.[9,23,31] The calculations were performed with the Γ-point regarding the large size of the used unit cell. The convergence parameters were set to 10^{-6} eV for the total energy and 0.02 eV $Å^{-1}$ for the atomic forces.

The interaction energies between the adsorbate and the zeolite have been evaluated according to the following equation: $E_{int} = E_{zeolite+X} - E_{zeolite} - E_X$, where $E_{zeolite+X}$ is the energy of the zeolite with the adsorbed molecules; $E_{zeolite}$ is the energy of the clean zeolite and E_X represents the energy of the molecule, which is put in the same box as for the system (zeolite + X) obtained after optimization.

Also, the dispersion energy contribution to the interaction energy was determined using the following equation: $E_{disp} = E_{disp\ zeolite+X} - E_{disp\ zeolite} - E_{disp\ X}$, where $E_{disp\ zeolite+X}$, $E_{disp\ zeolite}$ and $E_{disp\ X}$ are the dispersion contributions to the interaction energies of the zeolite with the adsorbed molecules, the clean zeolite and the isolated molecule in the gaseous phase, respectively. The optimized geometries are obtained after two steps: first, we have optimized the unit cell (without adsorbates) where we took into consideration the shape, atomic position and volume, and second, we have put the adsorbates in the zeolite, and then optimized the cell by relaxing only the atomic positions.

3 Results

3.1 Faujasite structure

Faujasite (FAU) belongs to the family of zeolites with large pores and has great thermal stability. The three-dimensional framework of FAU is mainly composed of sodalite cages (named also β cages) and supercages (named also α cages). The β cages with a diameter of 6.6 Å are connected to each other by a hexagonal prism (D6R).

The spherical α cages with a diameter of 12.4 Å are the source of the large pores in FAU and they are linked together *via* 12-membered ring windows with a diameter of 7.4 Å. Each supercage is connected to four other supercages and to four sodalite cages, and the access to the α cages from the β cages is possible *via* the hexagonal windows.[17,32]

Here, we have studied three faujasite structures with different Si/Al ratios of 47, 2.4 and 1.4, which correspond to silver loadings of 3.6 wt%, 34.5 wt% and 43 wt%, respectively. For the faujasite with a Si/Al ratio of 47 (the Ag-FAU(47) structure presented in Fig. 1), a Si atom is replaced by an Al atom and the charge produced from this change of atoms is compensated for by a Ag cation. For faujasite Y which corresponds to a Si/Al ratio of 2.4 (the Ag-Y structure presented in Fig. 1), in this case 14 Si atoms are replaced by

Open Access Article. Published on 03 February 2022. Downloaded on 5/31/2023 10:42:03 AM.
This article is licensed under a Creative Commons Attribution-NonCommercial 3.0 Unported Licence.

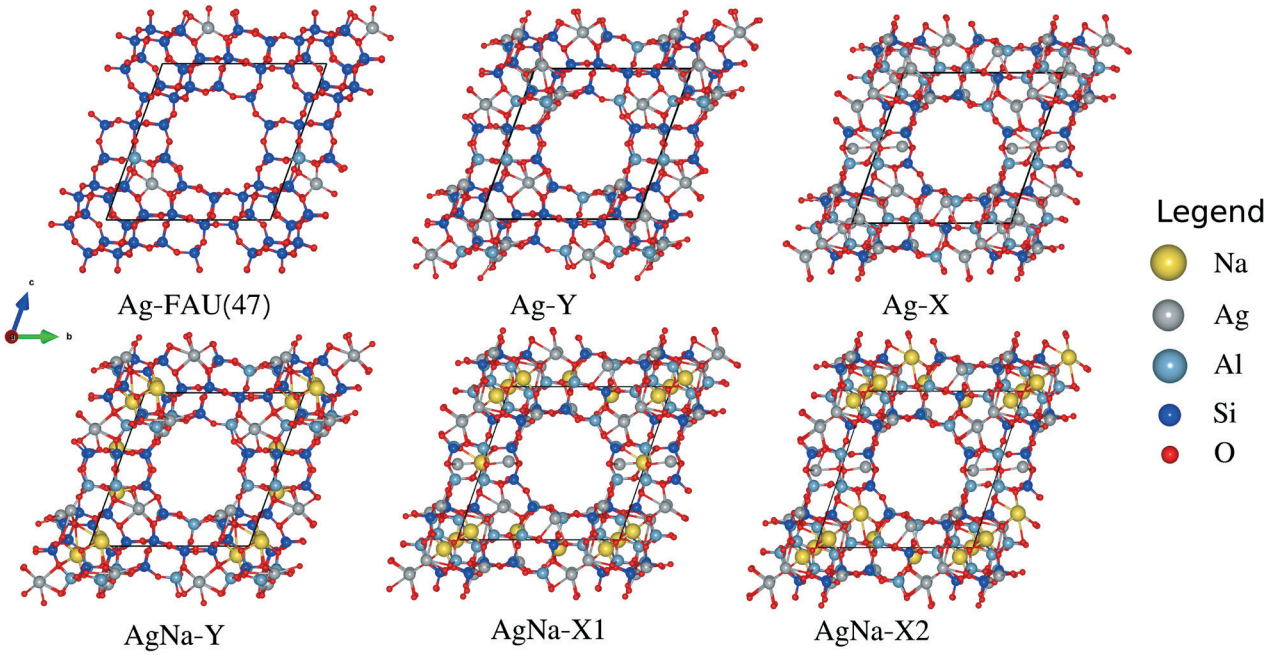

Fig. 1 Structural models of faujasite (FAU) projected along the *a* direction: the top panel presents the pure Ag-exchanged faujasite, while the bottom panel presents the AgNa-exchanged faujasite, with Si/Al ratios of 47(FAU(47)), 2.4(Y) and 1.4(X). The AgNa-X1 and AgNa-X2 labels correspond to the two different structures of AgNa-faujasite X. The spheres are just for illustration.

14 atoms of Al and to compensate for the charge induced in the Ag-Y model, 14 Ag cations are introduced. In the case of faujasite with a Si/Al ratio of 1.4 (named also X which corresponds to the Ag-X structure presented in Fig. 1), 20 cations of Ag are used to compensate for the charge induced from the replacement of 20 atoms of Si by 20 atoms of Al.

In Table 1, we present our computed interaction energies and the corresponding contribution of the dispersion energy of the different structures of faujasite. We found that the interactions between iodine species and the pure Ag-exchanged faujasite zeolites depend on the Si/Al ratios where the interaction energy of I_2 (CH_3I) is −107.7 kJ mol^{-1} (−117.7 kJ mol^{-1}) for Ag-FAU(47), −96.4 kJ mol^{-1} (−105.7 kJ mol^{-1}) in the case of Ag-Y, and −207.4 kJ mol^{-1} (−149.3 kJ mol^{-1}) in the case of Ag-X. Also, we found that the interaction energy for I_2 presents a significant increase in the case of Ag-X, which is related to a spontaneous dissociation of this molecule. Indeed, the CH_3I molecule is more adsorbed than I_2 by an energy amount (in terms of absolute value) of about 10 kJ mol^{-1} for FAU(47) and 9.3 kJ mol^{-1} for Ag-Y, while in the case of Ag-X, the observation is reversed where I_2 is more adsorbed than CH_3I by about 58.1 kJ mol^{-1}. Besides, we found that the dispersion contribution of both I_2 and CH_3I to their total interaction energies presents almost the same values independent of the Si/Al ratios. For the CO, H_2O and CH_3Cl molecules, we found that they present a similar trend to CH_3I where their interaction energies increase when the Si/Al ratio decreases to 1.4 (the case of Ag-X). In contrast, the molecule of Cl_2 presents a similar trend to I_2 where a spontaneous dissociation is obtained in the case of Ag-X, which leads to a considerable increase of the interaction energy.

For an efficient comparison of the performance of the different structures of faujasite, we used the radar charts presented in Fig. 2 where the best result is represented by the outermost ring.

We note that the results are put to zero when the inhibitor compounds are more adsorbed than the iodine species. In Fig. 2(a), we present the performance for the selective trapping of iodine species towards H_2O, CO, CH_3Cl and Cl_2

Table 1 Calculated interaction energies ΔE_{int} (kJ mol^{-1}) for CH_3I, I_2, CO, H_2O, CH_3Cl and Cl_2 in Ag- and NaAg-faujasite with Si/Al ratios of 47, 2.4 and 1.4. The contribution of the dispersion energy ΔE_{disp} (kJ mol^{-1}) to the interaction energies is given in parentheses

	Si/Al = 47	Si/Al = 2.4 (Y)		Si/Al = 1.4 (X)		
	Ag-FAU(47)	Ag-Y	AgNa-Y	Ag-X	AgNa-X1	AgNa-X2
CH_3I	−117.7 (−26.9)	−105.7 (−27.3)	−100.8 (−26.2)	−149.3 (−28.5)	−149.4 (−28.2)	−149.5 (−33.0)
I_2	−107.7 (−32.9)	−96.4 (−34.3)	−91.5 (−32.0)	−207.4 (−30.5)	−202.6 (−35.9)	−195.3 (−30.5)
CO	−114.4 (−9.1)	−94.0 (−9.1)	−99.5 (−9.1)	−152.6 (−10.8)	−154.4 (−10.1)	−153.7 (−11.8)
H_2O	−70.0 (−7.7)	−68.6 (−9.0)	−65.5 (−7.8)	−111.6 (−11.7)	−113.4 (−11.9)	−114.1 (−12.5)
CH_3Cl	−82.7 (−21.7)	−72.0 (−21.3)	−74.11 (−21.32)	−114.4 (−22.6)	−114.4 (−22.5)	−113.1 (−25.7)
Cl_2	−59.6 (−19.6)	−45.0 (−18.3)	−45.5 (−18.0)	−190.8 (−18.2)	−192.5 (−13.1)	−159.1 (−17.6)

 This journal is © The Royal Society of Chemistry and IChemE 2022

Open Access Article. Published on 03 February 2022. Downloaded on 5/31/2023 10:42:03 AM.
This article is licensed under a Creative Commons Attribution-NonCommercial 3.0 Unported Licence.

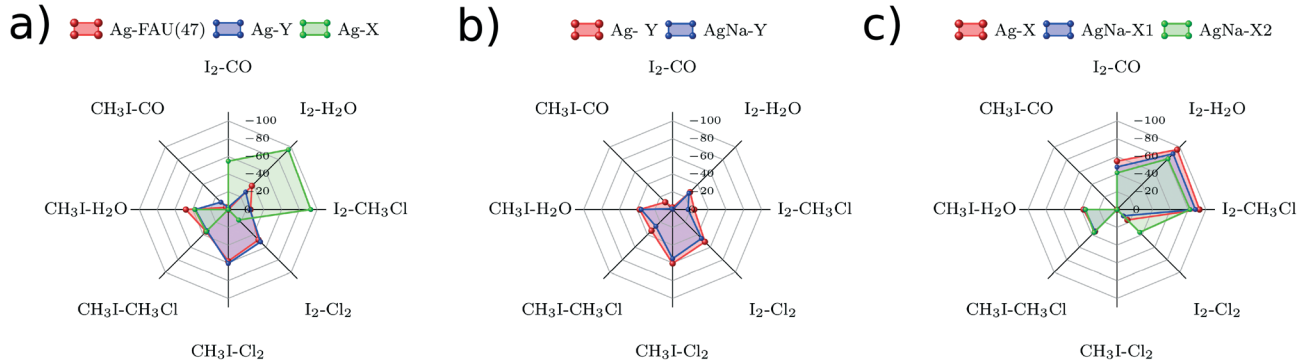

Fig. 2 Radar charts comparing the difference in interaction energies between iodine species (I_2 and CH_3I) and M molecules (M = CO, H_2O, CH_3Cl and Cl_2) adsorbed on (a) Ag-faujasite, (b) Ag/AgNa-Y and (c) Ag/AgNa-X.

of the pure silver exchanged FAU with Si/Al ratios of 47, 2.4 and 1.4, which correspond to the FAU(47), Ag-Y and Ag-X structures, respectively. Globally, we can see that the area covered by Ag-X is larger than that covered by Ag-FAU(47) and Ag-Y. Also, we observe that the FAU(47) and Ag-Y structures offer very comparative results where we found that the $I_2(CH_3I)$ molecule is more adsorbed (in terms of absolute value) than H_2O, CH_3Cl and Cl_2 by about 33 kJ mol^{-1} (45 kJ mol^{-1}), 25 kJ mol^{-1} (35 kJ mol^{-1}) and 48 kJ mol^{-1} (56 kJ mol^{-1}), respectively. On the contrary, a possible inhibiting effect is found with the CO molecule in the FAU(47) and Ag-Y zeolites, where the iodine species are weakly favored for adsorption by about 10 kJ mol^{-1}. On the other hand, we found that the Ag-X zeolite presents a different profile from those of FAU(47) and Ag-Y where I_2 is more adsorbed than H_2O, CO and CH_3Cl by an important amount of energy which can reach in absolute value: 95.8 kJ mol^{-1}, 54.8 kJ mol^{-1} and 92.8 kJ mol^{-1}, respectively. In contrast, I_2 is weakly favored for adsorption compared with Cl_2 by 16.6 kJ mol^{-1}. Also, we found that CH_3I is more adsorbed than the H_2O and CH_3Cl molecules by 37.7 kJ mol^{-1} and 34.9 kJ mol^{-1}, respectively, while Cl_2 and CO have similar interaction energies to CH_3I and therefore could inhibit its adsorption. All in all, we found that the I_2 molecule can be selectively adsorbed in faujasite X (see Fig. 2).

In order to use a smaller amount of silver which is an expensive metal, we have considered partially exchanged zeolites with Na cations in addition to Ag ones, to compensate for the charge in the Ag-Y and Ag-X structures. Previous experimental studies[24,33] on the faujasite structure (exchanged with Na and Ag cations) revealed that Ag cations mainly occupy sites SII and, to a lesser extent, sites SIII, both being located in the supercages.[34] Accordingly, we put the Ag cations in the supercages and the Na cations in the sodalite cages, which is the case of the AgNa-Y and AgNa-X1 structures. Then, we put the Na cations with the Ag cations in the supercages, while the sodalite cages are still occupied just by the Na cations, which corresponds to the AgNa-X2 model.

In these cases, the amount of silver decreases from 34.5 wt% to 21.5 wt% and from 43 wt% to 32 wt% in the cases of the Ag-Y and AgNa-X1(AgNa-X2) structures, respectively. The different structures are presented in Fig. 1.

Regarding the interaction energies and the corresponding contributions of the dispersion energy presented in Table 1, we can observe that the addition of the Na cations has a small effect on the interactions between the iodine species and the AgNa-faujasite structures. In the case of AgNa-Y, we found that the total interaction energy of $I_2(CH_3I)$ increases slightly from −96.4 kJ mol^{-1}(−105.7 kJ mol^{-1}) to −91.5 kJ mol^{-1} (−100.8 kJ mol^{-1}), and CH_3I is still more adsorbed than I_2 as in the Ag-Y zeolite. Moreover, we found that the total interaction energies of H_2O and CH_3Cl present a slight increase of about 5 kJ mol^{-1}, while a decrease of about 5 kJ mol^{-1} and 0.5 kJ mol^{-1} is observed for CO and Cl_2, respectively. For the AgNa-X1 and AgNa-X2 structures, we found that the total interaction energies for CH_3I, CO, H_2O and CH_3Cl present very similar values, with and without Na, which are around −149 kJ mol^{-1}, −153 kJ mol^{-1}, −113 kJ mol^{-1} and −114 kJ mol^{-1}, respectively. For I_2, an increase in the total interaction energy of about 4.8 kJ mol^{-1} and 12.1 kJ mol^{-1} is obtained in the case of AgNa-X1 and AgNa-X2, respectively. Also, we observe that the addition of the Na cations has no significant effect on the adsorption of Cl_2 in the case of AgNa-X1, where a decrease of about 2 kJ mol^{-1} is observed, but not in the case of AgNa-X2, where an increase in the total interaction energy value of about 31.5 kJ mol^{-1} is obtained which limits the effect of Cl_2 on the adsorption of iodine species. With regard to the dispersion contribution, we observe that the addition of the Na cations in the Ag-Y and Ag-X structures has a very weak effect, where a variation in the values of around 5 kJ mol^{-1} is obtained in the extreme cases.

We turn now to the exploration of the effect of Na in the Ag-Y and Ag-X structures using the radar charts. In Fig. 2(b), we can observe that the profile obtained for AgNa-Y is very similar to that obtained for Ag-Y, but with a two-fold lower silver content (by about 12.5%). Also, we found that the presence of sodium in Ag-Y obstructs more strongly the adsorption of CH_3I in the presence of CO. In Fig. 2(c), we observe that the Ag-X, AgNa-X1 and AgNa-X2 structures offer comparable performances for the selective trapping of iodine

Open Access Article. Published on 03 February 2022. Downloaded on 5/31/2023 10:42:03 AM.
This article is licensed under a Creative Commons Attribution-NonCommercial 3.0 Unported Licence.

species towards H_2O, CH_3Cl and CO. Also, we can distinguish that CO has a similar interaction energy to CH_3I, even with the addition of Na atoms in the faujasite X, and therefore could inhibit its adsorption. On the other hand, we found that the Cl_2 molecule is being less adsorbed than I_2 by about 30 kJ mol^{-1} in the case of AgNa-X2. Finally, we found that the presence of the Na atoms in the AgNa-X2 structure has a positive impact on the limitation of the spontaneous dissociation of Cl_2 against I_2 but not against CH_3I.

3.2 Mordenite structure

Mordenite (MOR) is a three dimensional network which is formed by three different types of cavities: the main channel (MC), the side channel (SC), and the side pocket (SP). Along the *c*-axis, the MC is obtained from 12-membered rings stacked in a parallel array. The access to the SP from the MC is possible through 8-membered rings. The MC is characterized by a large aperture able to accommodate big molecules such as iodine molecules which makes this channel favored for the adsorption of this type of molecule compared to the SC and SP.[16,23,35]

In this study, the Ag exchanged MOR structures based on the structure optimized by Bučko *et al.*[36] are used, with the primitive monoclinic cell doubled in the *c*-direction, where its lattice parameters are $a = b = 13.805$ Å, $c = 15.212$ Å and $\beta = 82.81$. According to previous studies,[23] we have selected the T1-E site which is the most energetically stable site of the MC. Depending on the Si/Al ratio, we have studied three Ag-MOR structures with Si/Al ratios of 47, 11 and 5, which correspond to the Ag-MOR(47), Ag-MOR(11) and Ag-MOR(5) structures, respectively. The silver loading is 3.6 wt% in the case of Ag-MOR(47), 13.1 wt% for Ag-MOR(11) and 23.1 wt% in the case of Ag-MOR(5). The different structures are presented in Fig. 3.

In Table 2, we present the interaction energies and the corresponding contribution of the dispersion energy for CH_3I, I_2, CO, H_2O, CH_3Cl and Cl_2 in Ag-MOR. Our results show that the interactions between I_2 and the pure silver-MOR structures depend on the Si/Al ratio where the total interaction energy in absolute value increases from 132.6 kJ mol^{-1} for Si/Al = 47, to 183.8 kJ mol^{-1} in the case of Si/Al = 11, and then to 297.6 kJ mol^{-1} for Si/Al = 5. This increase obtained in the interaction energy values in the case of Si/Al ratios of 11 and 5, compared to the case of Si/Al = 47, is related to a spontaneous dissociation of I_2 where the I–I bond length is about 3.06 Å when Si/Al = 11, while it is about 4.54 Å when Si/Al = 5. On the other hand, we found that the interaction energy of CH_3I depends also on the Si/Al ratio where the values obtained are −152.1 kJ mol^{-1}, −151.8 kJ mol^{-1} and −188.5 kJ mol^{-1} in the cases of a Si/Al ratio of 47, 11 and 5, respectively. For the CO and H_2O molecules, we observe that the interaction energy values decrease with the decrease of Si/Al, while the values obtained for the CH_3Cl molecule present an increase with the decrease of Si/Al. For Cl_2, a similar observation to that for I_2 is obtained where an

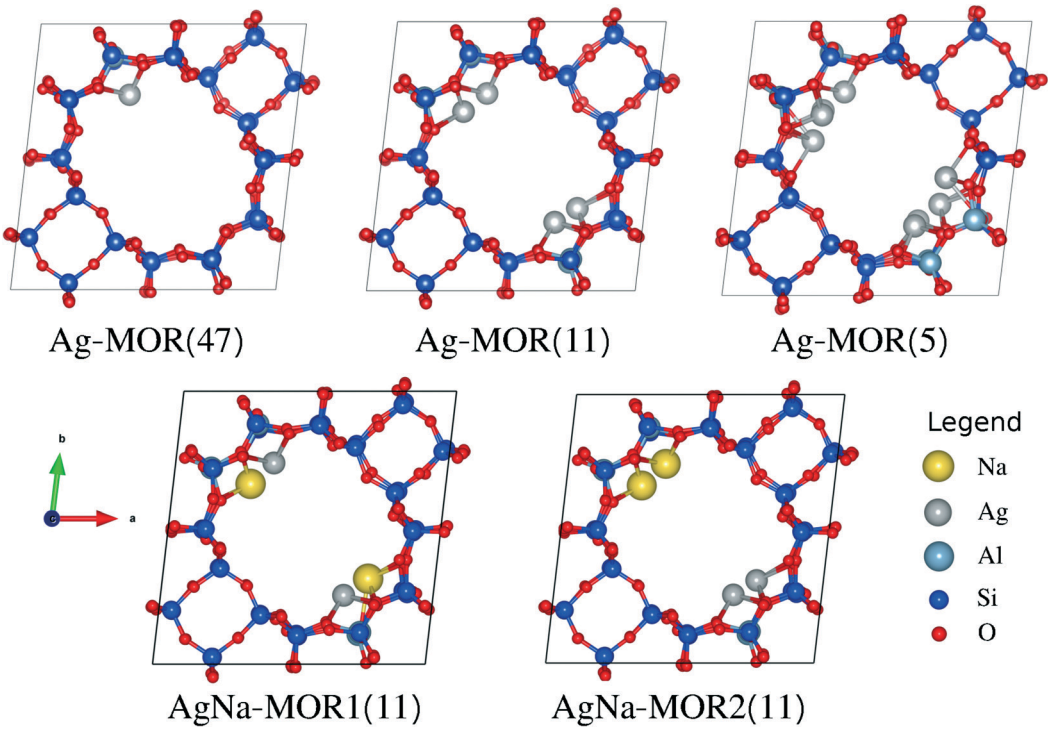

Fig. 3 Structural models of mordenite (MOR) projected along the *c* direction: the top panel presents the pure Ag-exchanged mordenite, while the bottom panel presents the AgNa-exchanged mordenite, with Si/Al ratios of 47(MOR(47)), 11(MOR(11)) and 5(MOR(5)). The AgNa-MOR1(11) and AgNa-MOR2(11) labels correspond to the two different models of AgNa-mordenite with a Si/Al ratio of 11. The spheres are just for illustration.

 This journal is © The Royal Society of Chemistry and IChemE 2022

Open Access Article. Published on 03 February 2022. Downloaded on 5/31/2023 10:42:03 AM.
This article is licensed under a Creative Commons Attribution-NonCommercial 3.0 Unported Licence.

Table 2 Calculated interaction energies ΔE_{int} (kJ mol^{-1}) for CH_3I, I_2, CO, H_2O, CH_3Cl and Cl_2 in Ag- and AgNa-mordenite, with Si/Al ratios of 47, 11 and 5. The contribution of the dispersion energy ΔE_{disp} (kJ mol^{-1}) to the interaction energies is given in parentheses

	Si/Al = 47	Si/Al = 11			Si/Al = 5
	Ag-MOR(47)	Ag-MOR(11)	AgNa-MOR1(11)	AgNa-MOR2(11)	Ag-MOR(5)
CH_3I	−152.1 (−36.2)	−151.8 (−41.4)	−128.8 (−39.5)	−139.9 (−40.2)	−188.5 (−50.9)
I_2	−132.6 (−46.0)	−183.8 (−42.9)	−154.3 (−45.7)	−155.9 (−47.4)	−297.6 (−56.0)
CO	−127.0 (−12.2)	−119.7 (−16.1)	−116.4 (−14.4)	−110.6 (−15.5)	−115.1 (−15.6)
H_2O	−111.5 (−10.4)	−90.3 (12.0)	−89.8 (−14.6)	−102.4 (−14.5)	−106.7 (−17.1)
CH_3Cl	−103.8 (−30.4)	−89.6 (−32.0)	−90.4 (−32.0)	−80.3 (−31.6)	−126.8 (−36.4)
Cl_2	−76.9 (−26.3)	−159.9 (−23.5)	−97.2 (−25.2)	−81.3 (−27.2)	−308.5 (−28.3)

increase in the interaction energies coupled with spontaneous dissociation is observed when the Si/Al ratio is 5 and 11. We can see that the capture mechanism of iodine species is more efficient with a low Si/Al ratio which is related to the size of molecules: the size of I_2 and CH_3I molecules is larger than the size of CO and H_2O, which make them more favorable to interact with more than a single cation. In contrast, related to their small size, the CO and H_2O molecules can interact just with a single cation.

In Fig. 4(a), we present the performance of the pure Ag-MOR(47), Ag-MOR(11) and Ag-MOR(5) for the selective trapping of iodine species towards H_2O, CO, CH_3Cl and Cl_2. It is seen that Ag-MOR(5) presents the outermost ring compared to Ag-MOR(47) and Ag-MOR(11). In the case of Ag-MOR(47), we found that I_2(CH_3I) is more adsorbed than H_2O, CH_3Cl and Cl_2 by about 21.1 kJ mol^{-1} (40.6 kJ mol^{-1}), 28.8 kJ mol^{-1} (48.3 kJ mol^{-1}) and 55.7 kJ mol^{-1} (75.2 kJ mol^{-1}), respectively. Indeed, CH_3I is also more adsorbed than CO by an important amount of energy of 25.1 kJ mol^{-1}, while I_2 is slightly more adsorbed than CO by about 5.6 kJ mol^{-1}, which can inhibit its adsorption. On the other hand, the Ag-MOR(5) and Ag-MOR(11) structures present good results for the selective trapping of iodine species towards CO, H_2O and CH_3Cl. In contrast, we found that Cl_2 can inhibit the adsorption of CH_3I in both Ag-MOR(5) and Ag-MOR(11) zeolites.

Then, we have considered partially exchanged zeolites with Na cations in addition to the Ag ones, to compensate for the charge in the MOR structure with a Si/Al ratio of 11. We studied two structures named hereafter as AgNa-MOR1(11) and AgNa-MOR2(11), as presented in Fig. 3. The silver loading decreases from 13.1 wt% in the case of Ag-MOR(11) to 6.5 wt% in the cases of AgNa-MOR1(11) and AgNa-MOR2(11).

Our computed interaction energies and the corresponding contribution of the dispersion energy of iodine species (I_2 and CH_3I) and M molecules (M = CO, H_2O, CH_3Cl and Cl_2) adsorbed on AgNa-MOR1(11) and AgNa-MOR2(11) are presented in Table 2. According to our results, the addition of the Na cations in Ag-MOR(11) decreases the total interaction energies (in absolute values) of CH_3I by about 23 kJ mol^{-1} and 11.9 kJ mol^{-1} in the cases of AgNa-MOR1(11) and AgNa-MOR2(11), respectively. Indeed, for the CO, H_2O and CH_3Cl molecules, we found that the most important impact obtained by the addition of Na cations is a decrease/increase in their interaction energy of about 10 kJ mol^{-1} in the extreme case. Interestingly, we found that the addition of Na prevents the dissociation of both I_2 and Cl_2 molecules but its impact on the interaction energy of Cl_2 is greater, where a decrease in the absolute values of the order of 62/78 kJ mol^{-1} is obtained, while a decrease in the order of 29.5/27.9 kJ mol^{-1} is obtained for I_2, in the case of AgNa-MOR1(11)/AgNa-

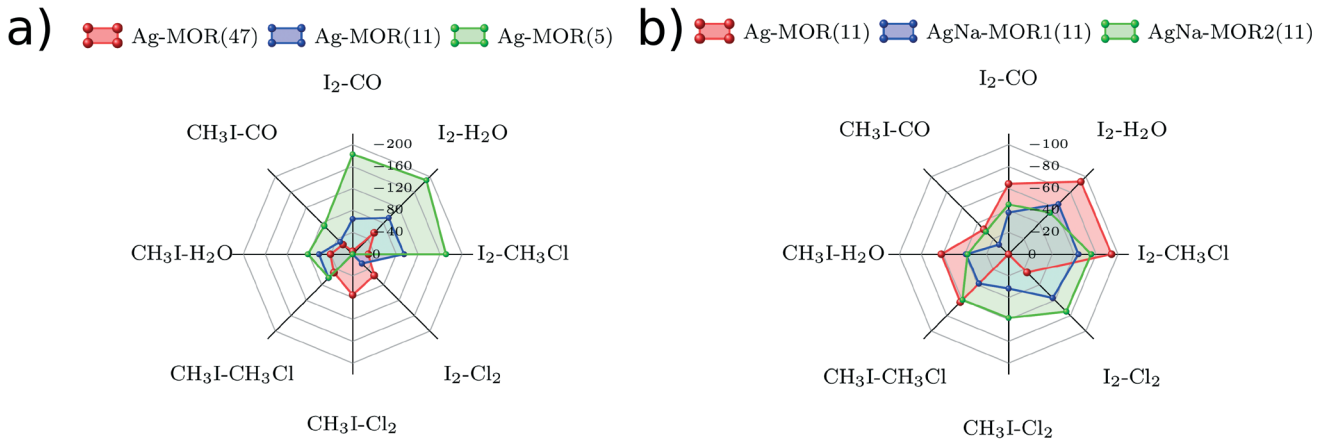

Fig. 4 Radar charts comparing the difference in interaction energies between iodine species (I_2 and CH_3I) and M molecules (M = CO, H_2O, CH_3Cl and Cl_2) adsorbed on (a) Ag-mordenite and (b) Ag/AgNa-mordenite with a Si/Al ratio of 11.

Open Access Article. Published on 03 February 2022. Downloaded on 5/31/2023 10:42:03 AM.
This article is licensed under a Creative Commons Attribution-NonCommercial 3.0 Unported Licence.

MOR2(11). Regarding the dispersion contribution, we found that they present almost the same values with and without Na, and independent of the Si/Al ratios.

To better understand the effect of the Na cations, we used the radar charts to compare the performance of Ag-MOR(11), AgNa-MOR1(11) and AgNa-MOR2(11) for the selective trapping of iodine species towards H_2O, CO, CH_3Cl and Cl_2, see Fig. 4(b). We can clearly observe that the problem obtained during the adsorption of CH_3I in the presence of Cl_2 is resolved with the addition of the Na cations where CH_3I is being more adsorbed than Cl_2 by around 31.6 kJ mol^{-1} in the case of AgNa-MOR1(11) and by around 58.6 kJ mol^{-1} in the case of AgNa-MOR2(11). Also, we observe that CO has a similar interaction energy to CH_3I and therefore could inhibit its adsorption in the case of AgNa-MOR1(11). Finally, we found that the presence of the Na cations presents a positive impact on the selective trapping of iodine species towards H_2O, CO, CH_3Cl and Cl_2 on the AgNa-MOR(11) structures, especially in the case of AgNa-MOR2(11).

3.3 Chabazite structure

Chabazite (CHA) is a three dimensional framework formed mainly by double six-ring prisms (6DR), four-membered rings (4MR) and eight-membered rings (8MR). The double six-ring prisms (6DR) arranged in layers are connected to each other by the tilted four-membered rings (4MR). The access to the crystal is possible from the 8MR which function as highly selective doorways with a diameter of 3.8 Å.[37–39] Here, we have studied three Ag-exchanged chabazite structures with Si/Al ratios of 23, 11 and 5, which correspond to the Ag-CHA(23), Ag-CHA(11) and Ag-CHA(5) structures (see Fig. 5), respectively. The silver loading is 7 wt% in the case of Ag-CHA(23), 23.1 wt% for Ag-CHA(11) and 23.1 wt% in the case of Ag-MOR(5).

Regarding the interaction energy values presented in Table 3, we found that the interactions between $I_2(CH_3I)$ and the CHA zeolites depend on the Si/Al ratio, where the interaction energy in absolute value increases from 124.2 kJ mol^{-1} (133.5 kJ mol^{-1}) for Si/Al = 23, to 158.3 kJ mol^{-1} (134.4 kJ mol^{-1}) in the case of Si/Al = 11, and to 190.6 kJ mol^{-1} (155.7 kJ mol^{-1}) for Si/Al = 5. We observe that the impact of the Si/Al ratio is more important in the case of I_2 than CH_3I, which is in line with the increase of the silver amount (decrease of the Si/Al ratio) coupled with the increase of the I–I bond-length, which is 2.71 Å for Si/Al = 23 and 2.80 Å for both Si/Al = 11 and 5. Also, we found that the interaction energy in absolute value of Cl_2 increases with the increase of the silver amount which is around 71 kJ mol^{-1} in the case of Si/Al = 23 and 11, and about 100.2 kJ mol^{-1} for Si/Al = 5. For CO, H_2O and CH_3Cl, a variation of about 5 kJ mol^{-1} is obtained in the interaction energy values as a function of the Si/Al ratio. Besides, we found that the dispersion

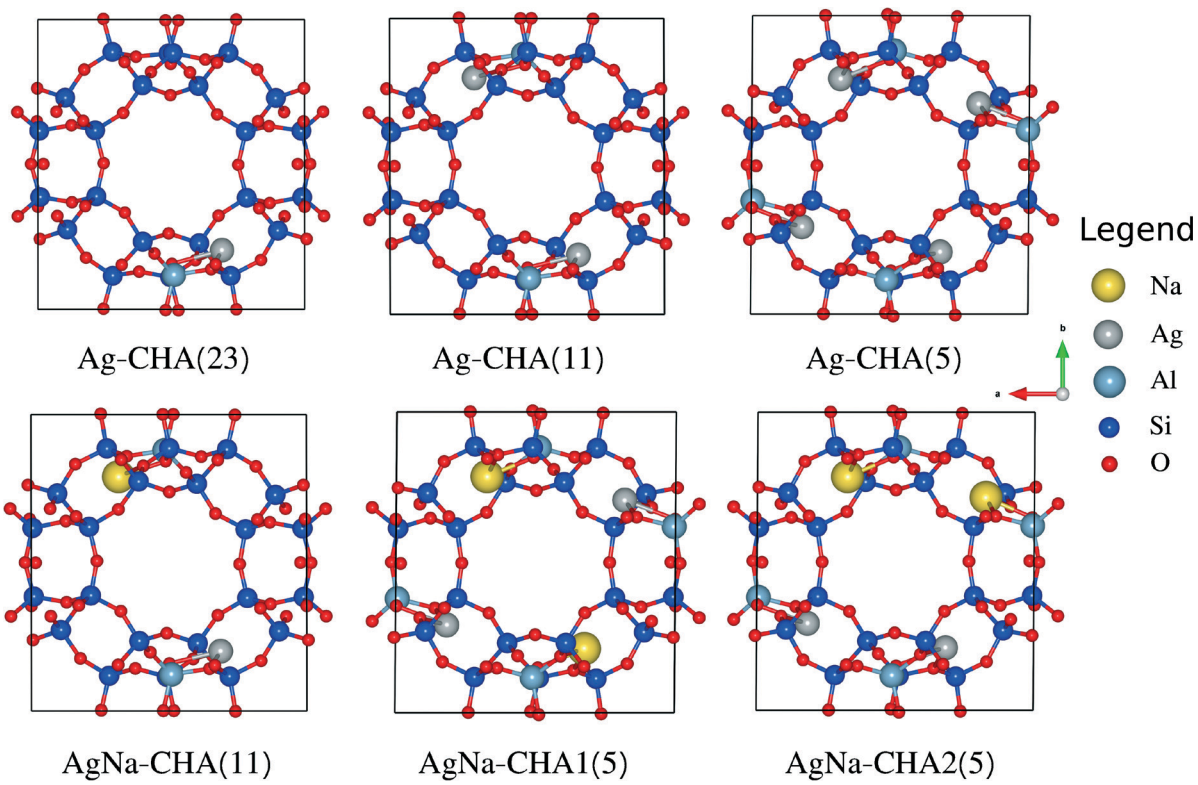

Fig. 5 Structural models of chabazite (CHA) projected along the *c* direction: the top panel presents the pure Ag-exchanged chabazite, while the bottom panel presents the AgNa-exchanged chabazite, with Si/Al ratios of 23(CHA(23)), 11(CHA(11)) and 5(CHA(5)). The AgNa-CHA1(5) and AgNa-CHA2(5) labels correspond to the two different models of AgNa-chabazite with a Si/Al ratio of 5. The spheres are just for illustration.

 This journal is © The Royal Society of Chemistry and IChemE 2022

Open Access Article. Published on 03 February 2022. Downloaded on 5/31/2023 10:42:03 AM.
This article is licensed under a Creative Commons Attribution-NonCommercial 3.0 Unported Licence.

Table 3 Calculated interaction energies ΔE_{int} (kJ mol^{-1}) for CH_3I, I_2, CO, H_2O, CH_3Cl and Cl_2 in Ag- and AgNa-chabazite, with Si/Al ratios of 23, 11 and 5. The contribution of the dispersion energy ΔE_{disp} (kJ mol^{-1}) to the interaction energies is given in parentheses

	Si/Al = 23	Si/Al = 11		Si/Al = 5		
	Ag-CHA(23)	Ag-CHA(11)	AgNa-CHA(11)	Ag-CHA(5)	AgNa-CHA1(5)	AgNa-CHA2(5)
CH_3I	−133.5 (−38.5)	−134.4 (−44.5)	−133.5 (−44.2)	−155.7 (−45.3)	−128.6 (−45.3)	−139.3 (−45.5)
I_2	−124.2 (−47.0)	−158.3 (−44.4)	−136.7 (−46.0)	−190.6 (−52.2)	−131.1 (−49.5)	−149.7 (−47.8)
CO	−126.5 (−16.1)	−124.7 (−16.5)	−124.3 (−16.4)	−129.8 (−16.8)	−118.5 (−15.5)	−119.1 (−47.8)
H_2O	−101.5 (−14.1)	−99.1 (−14.3)	−97.7 (−14.1)	−117.0 (−14.0)	−119.3 (−13.8)	−116.9 (−13.7)
CH_3Cl	−96.9 (−30.1)	−94.5 (−32.4)	−93.2 (−33)	−98.5 (−35.3)	−91.5 (−34.9)	−98.6 (−33.7)
Cl_2	−71.7 (−27.2)	−70.3 (−27.7)	−69.6 (−27.5)	−100.2 (−28.0)	−67.9 (−27.9)	−81.5 (−29.7)

contributions to the total interaction energies of the different molecules studied here present almost the same values, independent of the Si/Al ratio. For the chabazite structure, we found that the capture mechanism of iodine species depends on the Si/Al ratio where it is more efficient with the lower one.

Using the radar charts presented in Fig. 6(a), we found that the Ag-CHA(5) zeolite presents the best performance for trapping iodine species towards the M molecule (M = CO, H_2O, CH_3Cl and Cl_2) where it has the outermost ring compared to those of the Ag-CHA(23) and Ag-CHA(11) zeolites. We observe that Ag-CHA(11) and Ag-CHA(5) offer a good trapping of iodine species *versus* H_2O, CH_3Cl and Cl_2. In contrast, we found that CO has a similar interaction energy to iodine species and therefore could inhibit their adsorption in the case of Ag-CHA(11). In the case of the Ag-CHA(23) zeolite, it is seen that the area occupied by this structure is the smallest compared to those of the Ag-CHA(5) and Ag-CHA(11) zeolites, where we found that the CO and H_2O compounds can exhibit an inhibiting effect for the adsorption of iodine species.

With the addition of Na cations together with Ag ones, to compensate for the charge in the Ag-CHA(11) and Ag-CHA(5) zeolites, we studied three structures which are AgNa-CHA(11) with a Si/Al ratio of 11, and AgNa-CHA1(5) and AgNa-CHA2(5) with a Si/Al ratio of 5, as presented in Fig. 5. As per the results, the amount of silver decreases from 13.5 wt% to 6.5 wt% in the case of Si/Al = 11, and from 23.1 wt% to 12 wt% in the case of Si/Al = 5.

In Table 3, we present our computed interaction energies and the corresponding contribution of the dispersion energy for CH_3I, I_2, CO, H_2O, CH_3Cl and Cl_2 in AgNa-CHA(11), AgNa-CHA1(5) and AgNa-CHA2(5). For AgNa-CHA(11), we found that the addition of Na has a small effect on the interaction between CH_3I, CO, H_2O, CH_3Cl and Cl_2, and the CHA zeolite, where a decrease/increase of around 3 kJ mol^{-1} in the interaction energy values is obtained, compared to those obtained in the case of pure exchanged CHA with Si/Al = 11. In contrast, we found that the interaction energy in absolute value of I_2 decreases by about 21.6 kJ mol^{-1} with the decrease of silver loading, coupled with a weak decrease of the I–I bond length which is 2.8 Å for Ag-CHA(11) and 2.77 Å for AgNa-CHA(11). In the case of AgNa-CHA1(5) and AgNa-CHA2(5)s, we found that the interactions between $I_2(CH_3I)$ are affected by the presence of Na atoms in the zeolites where a decrease in the interaction energy in absolute value of around 59.5 kJ mol^{-1} (27.1 kJ mol^{-1}) and 40.9 kJ mol^{-1} (16.4 kJ mol^{-1}) is obtained in the case of AgNa-CHA1(5) and AgNa-CHA2(5), respectively. For the CO, H_2O and CH_3Cl molecules, we found that the most important impact obtained by the addition of Na cations is a decrease in their interaction energy values of about 10 kJ mol^{-1}, in the extreme case. In contrast, the effect of Na atoms is more important for the adsorption of the Cl_2 molecule where it is less adsorbed by around 32.3 kJ mol^{-1} (18.7 kJ mol^{-1}) in the case of AgNa-CHA1(5) (AgNa-CHA2(5)). Here, we observe that the addition of Na strongly influences the interaction energy of I_2 and Cl_2 compared to those of CH_3I, CO, H_2O and CH_3Cl. With regard

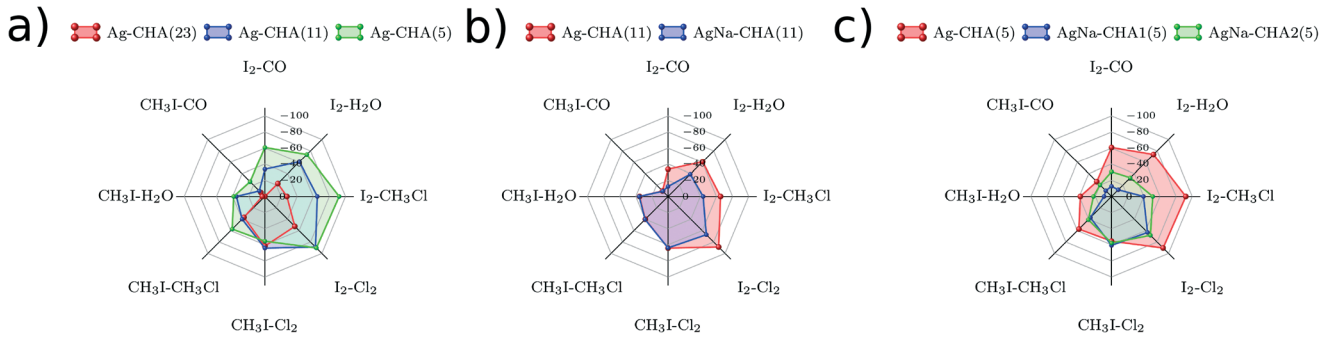

Fig. 6 Radar charts comparing the difference in interaction energies between iodine species (I_2 and CH_3I) and a M molecule (M = CO, H_2O, CH_3Cl and Cl_2) adsorbed on (a) Ag-chabazite and Ag/AgNa-chabazite with Si/Al ratios of (b) 11 and (c) 5.

Open Access Article. Published on 03 February 2022. Downloaded on 5/31/2023 10:42:03 AM.
This article is licensed under a Creative Commons Attribution-NonCommercial 3.0 Unported Licence.

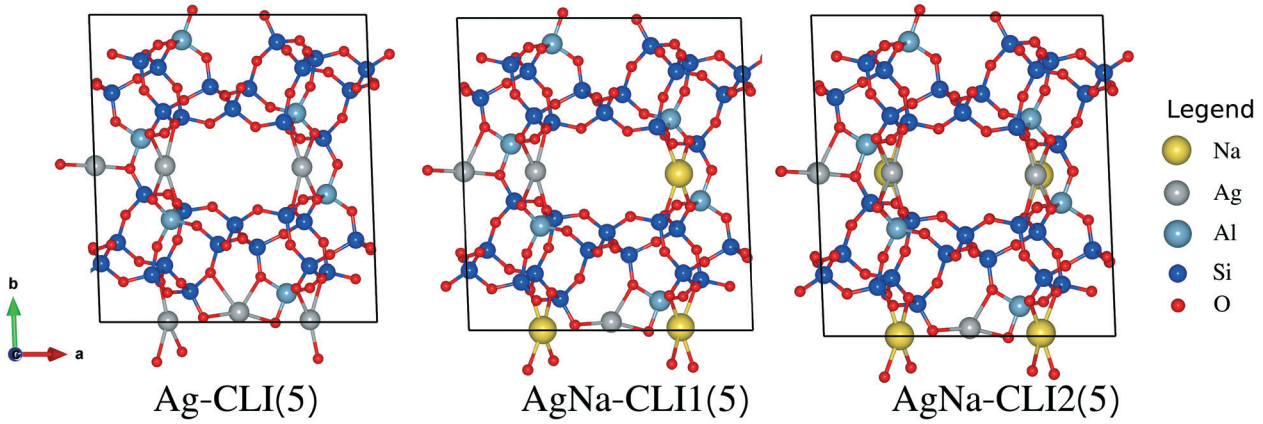

Fig. 7 Structural models of clinoptilolite (CLI), with a Si/Al ratio of 5, projected along the *c* direction: the left panel presents the pure Ag-exchanged clinoptilolite, while the middle and right panels present the AgNa-exchanged clinoptilolite. The AgNa-CLI1(5) and AgNa-CLI2(5) labels correspond to the two different structures of AgNa-clinoptilolite. The spheres are just for illustration.

to the mode of adsorption, we found that CH_3I, CO, H_2O and CH_3Cl interact only with the Ag atoms for the adsorption on AgNa-CHA(5), and they are not bound to the Na atoms; so here the main factor of the variation in the interaction energy for these molecules is the decrease in the silver loading. For I_2 and Cl_2, we found that the decrease in the interaction energy values is related not only to the silver loading, as for CH_3I, but also to the mode of adsorption where we found that the $I_2(Cl_2)$ molecule interacts with Ag atoms in the first side and with Na atoms in the second side, in some cases.

To better understand the effect of the addition of Na cations in the chabazite structures, we show in Fig. 6 the results obtained for selective trapping of iodine species in Ag-CHA(11) and AgNa-CHA(11) in the form of radar charts. In Fig. 6(b), we see that the Ag-CHA(11) and AgNa-CHA(5) zeolites offer a good performance for trapping I_2 and CH_3I towards H_2O, CH_3Cl and Cl_2. In contrast, CO presents an inhibiting effect on the adsorption of iodine compounds in Ag-CHA(11) even with the presence of Na atoms.

In Fig. 6(c), it is seen that the addition of Na cations decreases the area occupied by Ag-CHA(5). Despite the decrease in the area occupied by AgNa-CHA1(5) compared to that occupied by Ag-CHA(5), we found that AgNa-CHA1(5) offers a good trapping of iodine species towards H_2O, CO, CH_3Cl and Cl_2, with a lower silver content of around 11.1 wt%. On the other hand, we observe in the case of AgNa-CHA2(5) that H_2O and CO have similar interaction energies with iodine compounds and therefore could inhibit their adsorption.

3.4 Clinoptilolite structure

Clinoptilolite (CLINO) is characterized by a monoclinic structure and is one of the most common natural zeolites which is easily obtained from mines. CLINO is basically made up of three main channels A, B and C, where A and B run parallel to the *c*-axis, while C runs parallel to the *a*-axis and the [100] direction. Channels A and B are occupied by six cations at positions M1 and M2.[38,40–42] In this study, we used the unit cell suggested by Ruiz-Salvador *et al.*,[43] where its lattice parameters are a = 17.619 Å, b = 17.805 Å and c = 7.374 Å, and its cell angle β is 116.21°. In order to lodge the iodine compounds, our calculations are performed in the monoclinic supercell doubled in the *c*-direction. With a Si/Al ratio of 5, we have studied the pure Ag-exchanged CLINO structure, where the silver loading is about 23.1 wt%. In order to decrease the amount of silver, we introduced the Na cations in parallel with the Ag ones in the CLINO zeolite where we have studied two structures, which are AgNa-CLINO1(5) and AgNa-CLINO2(5), with an amount of silver of about 12.7 wt%, see Fig. 7.

Regarding the interaction energy values presented in Table 4, we found that the total interaction energies of I_2 and CH_3I are about −105.3 kJ mol^{-1} and −104.4 kJ mol^{-1}, respectively. On the other hand, H_2O, CO, CH_3Cl and Cl_2 are less adsorbed than the iodine species where their interaction energy values are −81.6, −88.3, −72.4 and −58.4 kJ mol^{-1}, respectively. With the addition of Na cations, we found that I_2, CH_3I, CO, CH_3Cl and Cl_2 are less adsorbed by around 5 kJ mol^{-1} in the case of AgNa-CLI(5) compared to Ag-CLI(5). In contrast, H_2O is more adsorbed by about 20 kJ mol^{-1} with the presence of Na cations, which makes it more adsorbed than iodine species. In regard to the contributions of dispersion energy to the interaction energies, we found that

Table 4 Calculated interaction energies ΔE_{int} (kJ mol^{-1}) for CH_3I, I_2, CO, H_2O, CH_3Cl and Cl_2 in Ag- and AgNa-clinoptilolite, with a Si/Al ratio of 5. The contribution of the dispersion energy ΔE_{disp} (kJ mol^{-1}) to the interaction energies is given in parentheses

	Ag-CLI(5)	AgNa-CLI1(5)	AgNa-CLI2(5)
CH_3I	−104.4 (−65.8)	−99.9 (−65.8)	−100.6 (−66.0)
I_2	−105.3 (−70.7)	−90.5 (−70.3)	−90.3 (−70.4)
CO	−88.3 (−26.0)	−84.9 (−26.6)	−84.1 (−26.6)
H_2O	−81.6 (−19.6)	−101.5 (−21.4)	−101.3 (−20.4)
CH_3Cl	−72.4 (−53.0)	−70.9 (−51.3)	−69.8 (−51.6)
Cl_2	−58.4 (−47.2)	−55.0 (−45.7)	−45.9 (−45.9)

 This journal is © The Royal Society of Chemistry and IChemE 2022

Open Access Article. Published on 03 February 2022. Downloaded on 5/31/2023 10:42:03 AM.
This article is licensed under a Creative Commons Attribution-NonCommercial 3.0 Unported Licence.

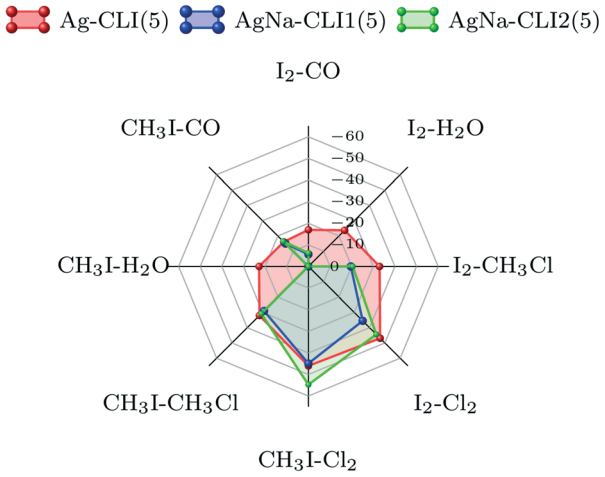

Fig. 8 Radar charts comparing the difference in interaction energies between iodine species (I_2 and CH_3I) and M molecules (M = CO, H_2O, CH_3Cl and Cl_2) adsorbed on Ag- and AgNa-clinoptilolite.

they are not significantly influenced by the addition of Na cations.

In Fig. 8, we observe that the Ag-CHA(5) structure offers the best performance for trapping iodine species, compared to AgNa-CLI1(5) and AgNa-CLI2(5), which is presented by the larger area. On the other hand, we see that the profiles of AgNa-CLI1(5) and AgNa-CLI2(5) are similar, where we found that H_2O and CO have a similar interaction energy to the iodine species, which can inhibit their adsorption.

4 Discussion

As described in previous sections, the spontaneous dissociation of the molecules I_2 and Cl_2 considerably increases their interaction energies with zeolite. In fact, this increase in energy is very important in the case of I_2 which makes it privileged in adsorption *versus* most of the molecules studied here. In contrast, the spontaneous dissociation of Cl_2 has a negative impact since it favours the adsorption of this molecule against the iodine species, in particular CH_3I. Also, we found that the dissociation of I_2 and Cl_2 depends on the distance between the Ag atoms interacting with the I(Cl) atom on each side of their molecule. In Fig. 9, the interaction energy is presented as a function of the average distance '*d*' between Ag cations which interact with $I_2(Cl_2)$ during the adsorption. Here, we aim to decouple the spontaneous dissociation observed in parallel for I_2 and Cl_2 where we are looking to find a Ag–Ag distance which increases the adsorption of I_2 and at the same time avoids the spontaneous dissociation of Cl_2. We can observe that I_2 and Cl_2 have similar interaction energy values where a spontaneous dissociation is seen in the cases of Ag-X, Ag-MOR(11) and Ag-MOR(5). On the other hand, we found that I_2 is more adsorbed than Cl_2 by an important amount of energy, which is around 90.4 kJ mol^{-1}, 88.7 kJ mol^{-1} and 46.9 kJ mol^{-1} for Ag-CHA(5), Ag-CHA(11) and Ag-CLI(5), respectively. In these last cases, we note that no spontaneous dissociation of I_2 and Cl_2 is obtained but an increase in the I–I (Cl–Cl) bond length is observed which is 2.8 Å(2.25 Å) for Ag-CHA(5), 2.8 Å(2.03 Å) in the case of Ag-CHA(11) and 2.7 Å(2.0 Å) for Ag-CLI(5). We note that our optimized I–I (Cl–Cl) bond length in the gas phase with TS/HI is 2.68 Å(1.99 Å). As per the results, we found that the suitable average Ag–Ag distances are about 7.04 Å and 9.53 Å, which are able to limit the dissociation of Cl_2 and improve the adsorption of I_2.

In Fig. 10, we present the radar charts to compare the results obtained for the Ag-CLI(5), AgNa-Y, AgNa-MOR2(11) and Ag-CHA(5) zeolites. The Ag-CHA(5) and AgNa-MOR2(11) zeolites offer the best results for the selective trapping of I_2 towards CO, H_2O, CH_3Cl and Cl_2 compared to others; AgNa-Y and Ag-CLI(5), this trend is less marked for CH_3I. Regarding the silver amount in structures, we found that AgNa-MOR2(11) with 6.5 without 10 wt% of silver loading is required to get good performance.

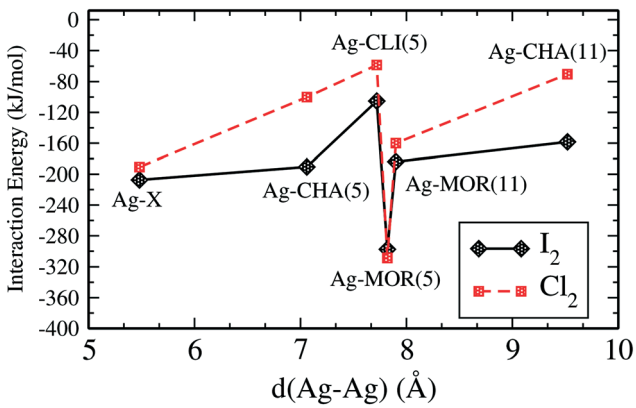

Fig. 9 Interaction energy as a function of the average distance *d*(Ag–Ag) for Ag-exchanged zeolites. The black line corresponds to the I_2 interaction energy, while the red line corresponds to the Cl_2 interaction energy.

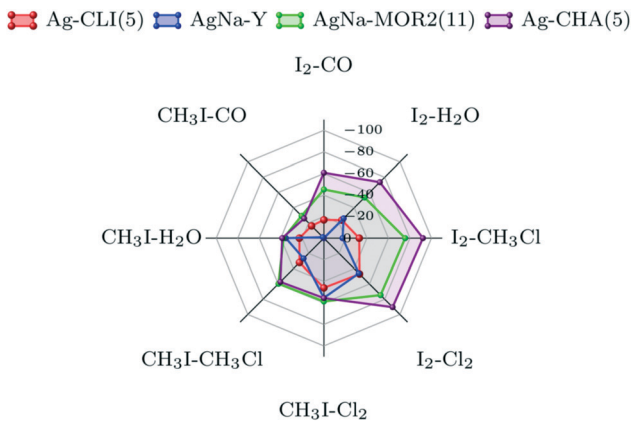

Fig. 10 Radar charts comparing the difference in interaction energies between iodine species (I_2 and CH_3I) and M molecules (M = CO, H_2O, CH_3Cl and Cl_2) adsorbed on Ag- and AgNa-zeolites.

Open Access Article. Published on 03 February 2022. Downloaded on 5/31/2023 10:42:03 AM.
This article is licensed under a Creative Commons Attribution-NonCommercial 3.0 Unported Licence.

Table 5 Calculated interaction energies ΔE_{int} (kJ mol^{-1}) and distances (Ag–I) for I_2, CH_3I, I_2 + CO/H_2O and CH_3I + CO/H_2O in AgNa-Y. The interaction energies given in parentheses present the sum of the interaction energies of isolated molecules

	E_{int} (kJ mol^{-1})	d(Ag–I) (Å)
2 I_2	−187.1 (−183.0)	2.62
I_2 +H_2O	−139.7 (−157.0)	2.72
I_2 + CO	−163.3 (−191.0)	2.83
2 CH_3I	−173.7 (−201.6)	2.64
CH_3I + H_2O	−162.8 (−166.3)	2.67
CH_3I + CO	−139.2 (−200.3)	2.88

Here, we discuss the effect of the adsorption of a second iodine species, and the co-adsorption of inhibitor compounds (CO and H_2O) with iodine species (I_2 and CH_3I) for the less efficient case AgNa-Y (see Fig. 10). In Table 5, we present the calculated interaction energies ΔE_{int} (kJ mol^{-1}) and distances (Ag–I) for 2 I_2, 2 CH_3I, I_2 + CO/H_2O and CH_3I + CO/H_2O in the AgNa-Y structure. We found that the adsorption of a second iodine species has almost no effect on the adsorption of the first iodine molecule on a specific cation. Indeed, the interaction energy of 2 I_2 together is equivalent to the sum of the interaction energies of 2 I_2 alone. For the co-adsorption mechanism, we found that indeed there is a significant effect with a variation of the interaction energy values, depending on the molecule. Water has a small effect where a decrease in the interaction energy of about 17.3 kJ mol^{-1} and about 3.5 kJ mol^{-1} is obtained upon adsorption with I_2 and CH_3I, respectively (see Table 5). Together with this small decrease in the interaction energy, a small increase in the Ag–I distance of about 0.1 Å is observed upon the adsorption of H_2O with iodine molecules. In contrast, we found that CO presents a significant effect where a decrease in the interaction energy of about 27.7 kJ mol^{-1} and 60.8 kJ mol^{-1} is obtained upon adsorption with I_2 and CH_3I, respectively. Also, this strong effect of CO appears in the Ag–I distance where an increase of about 0.2 Å is observed in both cases. Finally, we see that the adsorption of CH_3I is more perturbed than I_2 by the presence of CO.

5 Conclusion

In summary, we have investigated the selective trapping of iodine species *versus* H_2O, CO, CH_3Cl and Cl_2 for four different zeolites which are faujasite, mordenite, chabazite and clinoptilolite. For the faujasite structure, we found that the results obtained depend on the Si/Al ratio where a better selective trapping of iodine compounds in comparison with H_2O and CH_3Cl is obtained with Si/Al = 1.4 (X structure), while a better selective trapping of iodine compounds in comparison with Cl_2 is obtained with Si/Al = 47 and 2.4 (Y structure). In contrast, we found that faujasite is not suitable for the selective trapping of iodine species towards CO, independent of the Si/Al ratio. In the case of mordenite, CO is expected to present an inhibiting effect on the adsorption of iodine compounds with a Si/Al ratio of 47. Going from a Si/Al ratio of 47 to 11 and 5, the CO inhibitory effect has disappeared but we found that Cl_2 is expected to present an inhibiting effect. On the other hand, we found that the addition of the Na cations in mordenite with Si/Al = 11 improved its performance in the selective trapping of iodine compounds and a positive impact is observed in the limitation of the spontaneous dissociation of Cl_2. For chabazite, it has been shown that the pure Ag-exchanged structure with a Si/Al of 5 presents the best results for selective trapping of iodine species where an inhibiting effect is observed. In contrast, CO is expected to present an inhibiting effect on the adsorption of CH_3I for Si/Al = 23 and 11. In the case of clinoptilolite, we found that the pure Ag-exchanged structure offers the best performance compared with the other AgNa-exchanged structures. These results could be confirmed by experiments to get relevant data considering representative molar ratios of the gas involved and the shape of the potential porous material in considering the filtering efficiency requirement.

Conflicts of interest

There are no conflicts of interest to declare.

Acknowledgements

This work was granted access to the HPC resources of TGCC under the allocation 2021-A0100810433 by GENCI -EDARI project, and was supported by the French research program ANR-11-RSNR-0013-01 called MiRE (Mitigation of Iodine Releases in the Environment).

References

1 J. R. Brian, D. V. John, M. S. Denis, S. M. John and L. J. James, *J. Nucl. Mater.*, 2016, **470**, 307–326.
2 A. J. González, *Health Phys.*, 2007, **93**, 571.
3 M. Chebbi, B. Azambre, C. Monsanglant-Louvet, B. Marcillaud, A. Roynette and L. Cantrel, *J. Hazard. Mater.*, 2021, **409**, 124947.
4 J. Jolley and H. Tompkins, *Appl. Surf. Sci.*, 1985, **21**, 288–296.
5 K. W. Chapman, P. J. Chupas and T. M. Nenoff, *J. Am. Chem. Soc.*, 2010, **132**, 8897–8899.
6 L. N. Rastunov, E. P. Magomedbekov, A. V. Obruchikov and L. A. Lomazova, *At. Energy*, 2011, **110**, 68.
7 T. M. Nenoff, M. A. Rodriguez, N. R. Soelberg and K. W. Chapman, *Microporous Mesoporous Mater.*, 2014, **200**, 297–303.
8 S. U. Nandanwar, K. Coldsnow, V. Utgikar, P. Sabharwall and D. Eric Aston, *Chem. Eng. Sci.*, 2016, **306**, 369–381.
9 H. Jabraoui, E. Hessou, S. Chibani, L. Cantrel, S. Lebègue and M. Badawi, *Appl. Surf. Sci.*, 2019, **485**, 56–63.
10 L. E. Herranz, T. Lind, K. Dieschbourg, E. Riera, S. Morandi, P. Rantanen, M. Chebbi and N. Losch, *OECD REPORTRN: 47070575*, 2013, p. 2846.

 This journal is © The Royal Society of Chemistry and IChemE 2022

Open Access Article. Published on 03 February 2022. Downloaded on 5/31/2023 10:42:03 AM.
This article is licensed under a Creative Commons Attribution-NonCommercial 3.0 Unported Licence.

11 D. Jacquemain, S. Guentay, S. Basu, M. Sonnenkalb, L. Lebel, H.-J. Allelein, B. Liebana, B. Eckardt and L. Ammirabile, *OECD Report-RN:45089842*, 2014, p. 174.
12 J. Foit, *Nucl. Eng. Des.*, 1997, **170**, 73–79.
13 A. Auvinen, R. Zilliacus and J. Jokiniemi, *Nucl. Technol.*, 2005, **149**, 232–241.
14 M. Kitamura, K. Funabashi, M. Kikuchi, H. Yusa, Y. Fukushima and S. Horiuchi, Silver-impregnated alumina for removal of radioactive methyl iodide, *Trans. Am. Nucl. Soc.*, 1978, vol. 30, https://www.osti.gov/biblio/6537164.
15 D. F. Sava, M. A. Rodriguez, K. W. Chapman, P. J. Chupas, J. A. Greathouse, P. S. Crozier and T. M. Nenoff, *J. Am. Chem. Soc.*, 2011, **133**, 12398–12401.
16 S. Chibani, M. Chebbi, S. Lebègue, L. Cantrel and M. Badawi, *Phys. Chem. Chem. Phys.*, 2016, **18**, 25574–25581.
17 M. Chebbi, S. Chibani, J.-F. Paul, L. Cantrel and M. Badawi, *Microporous Mesoporous Mater.*, 2017, **239**, 111–122.
18 V. Van Speybroeck, K. Hemelsoet, L. Joos, M. Waroquier, R. G. Bell and C. R. A. Catlow, *Chem. Soc. Rev.*, 2015, **44**, 7044–7111.
19 E. R. Vance and D. K. Agrawal, *J. Mater. Sci.*, 1982, **17**, 1889.
20 R. T. Jubin, *Airborne waste management technology applicable for use in reprocessing plants for control of iodine and other off-gas constituents*, Report Number: ORNL/TM-10477, 1988, DOI: 10.2172/5169490.
21 B. S. Choi, G. I. Park, J. H. Kim, J. W. Lee and S. K. Ryu, *Adsorption*, 2001, **7**, 91.
22 Q. Cheng, Z. Li, T. Chu, W. Yang, Q. Zhu, D. He and C. Fang, *J. Radioanal. Nucl. Chem.*, 2015, **303**, 1883.
23 S. Chibani, M. Chebbi, S. Lebègue, T. Bucko and M. Badawi, *J. Chem. Phys.*, 2016, **144**, 244705.
24 B. Azambre and M. Chebbi, *ACS Appl. Mater. Interfaces*, 2017, **9**, 25194–25203.
25 T. Sun and K. Seff, *Chem. Rev.*, 1994, **94**, 857–870.
26 G. Kresse and D. Joubert, *Phys. Rev. B: Condens. Matter Mater. Phys.*, 1999, **59**, 1758.
27 G. Kresse and J. Hafner, *Phys. Rev. B: Condens. Matter Mater. Phys.*, 1993, **47**, 558.
28 J. P. Perdew, K. Burke and M. Ernzerhof, *Phys. Rev. Lett.*, 1996, **77**, 3865–3868.
29 F. Göltl, A. Grüneis, T. Bučko and J. Hafner, *J. Chem. Phys.*, 2012, **137**, 114111.
30 T. Bučko, S. Lebègue, J. Hafner and J. G. Ángyàn, *J. Chem. Theory Comput.*, 2013, **9**, 4293–4299.
31 T. Bučko, S. Lebègue, J. G. Ángyán and J. Hafner, *J. Chem. Phys.*, 2014, **141**, 034114.
32 E. Dempsey, G. H. Kuehl and D. H. Olson, *J. Phys. Chem.*, 1969, **73**, 387–390.
33 B. Azambre, M. Chebbi and A. Hijazi, *Chem. Eng. J.*, 2020, **379**, 122308.
34 T. Frising and P. Leflaive, *Microporous Mesoporous Mater.*, 2008, **114**, 27–63.
35 A. Alberti, P. Davoli and G. Vezzalini, *Z. Kristallogr. - Cryst. Mater.*, 1986, **175**, 249–256.
36 T. Bučko and J. Hafner, *J. Catal.*, 2015, **329**, 32–48.
37 C. Paolucci, A. A. Parekh, I. Khurana, J. R. Di Iorio, H. Li, J. D. Albarracin Caballero, A. J. Shih, T. Anggara, W. N. Delgass, J. T. Miller, F. H. Ribeiro, R. Gounder and W. F. Schneider, *J. Am. Chem. Soc.*, 2016, **138**, 6028–6048.
38 M. Abatal, A. R. Ruiz-Salvador and C. H. Norge, *Microporous Mesoporous Mater.*, 2020, **294**, 109885.
39 Y. Guo, T. Sun, Y. Gu, X. Liu, Q. Ke, X. Wei and S. Wang, *Chem. – Asian J.*, 2018, **13**, 3222–3230.
40 A. R. Ruiz-Salvador, A. Gómez, D. W. Lewis, C. R. A. Catlow, L. Marleny Rodríguez-Albelo, L. Montero and G. Rodríguez-Fuentes, *Phys. Chem. Chem. Phys.*, 2000, **2**, 1803–1813.
41 A. Rivera, T. Farías, L. C. de Ménorval, M. Autié-Pérez and A. Lam, *J. Phys. Chem. C*, 2013, **117**, 4079.
42 O. Korkuna, R. Leboda, J. Skubiszewska-Zieba, T. Vrublevska, V. Gunko and J. Ryczkowski, *Microporous Mesoporous Mater.*, 2006, **87**, 243–254.
43 A. R. Ruiz-Salvador, D. W. Lewis, J. Rubayo-Soneira, G. Rodríguez-Fuentes, L. R. Sierra and C. R. A. Catlow, *J. Phys. Chem. B*, 1998, **102**, 8417–8425.